The Astrophysical Journal, 887:171 (6pp), 2019 December 20 https://doi.org/10.3847/1538-4357/ab5585

X-Ray Observations of a $z \sim 6.2$ Quasar/Galaxy Merger

Thomas Connor[1,2], Eduardo Bañados[1,3], Daniel Stern[2], Roberto Decarli[4], Jan-Torge Schindler[3], Xiaohui Fan[5], Emanuele Paolo Farina[6], Chiara Mazzucchelli[7], John S. Mulchaey[1], and Fabian Walter[3,8]
[1] The Observatories of the Carnegie Institution for Science, 813 Santa Barbara St., Pasadena, CA 91101, USA; tconnor@carnegiescience.edu
[2] Jet Propulsion Laboratory, California Institute of Technology, 4800 Oak Grove Dr., Pasadena, CA 91109, USA
[3] Max Planck Institute for Astronomy, Königstuhl 17, D-69117 Heidelberg, Germany
[4] INAF—Osservatorio di Astrofisica e Scienza dello Spazio di Bologna, via Gobetti 93/3, I-40129, Bologna, Italy
[5] Steward Observatory, University of Arizona, 933 N. Cherry Ave., Tucson, AZ 85721, USA
[6] Max Planck Institut für Astrophysik, Karl-Schwarzschild-Straße 1, D-85748, Garching bei München, Germany
[7] European Southern Observatory, Alonso de Cordova 3107, Vitacura, Region Metropolitana, Chile
[8] National Radio Astronomy Observatory, Pete V. Domenici Array Science Center, P.O. Box O, Socorro, NM 87801, USA
Received 2019 September 18; revised 2019 November 5; accepted 2019 November 6; published 2019 December 18

Abstract

Quasars at early redshifts ($z > 6$) with companion galaxies offer unique insights into the growth and evolution of the first supermassive black holes. Here, we report on a 150 ks *Chandra* observation of PSO J308.0416−21.2339, a $z = 6.23$ quasar with a merging companion galaxy identified in [C II] and rest-frame UV emission. With $72.3^{+9.6}_{-8.6}$ net counts, we find that PSO J308.0416−21.2339 is powerful ($L_X = 2.31^{+1.14}_{-0.76} \times 10^{45}$ erg s^{-1} cm^{-2} in rest-frame 2.0–10.0 keV) yet soft (spectral power-law index $\Gamma = 2.39^{+0.37}_{-0.36}$ and optical-to-X-ray slope $\alpha_{OX} = -1.41 \pm 0.11$). In addition, we detect three hard-energy photons 2.″0 to the west of the main quasar, cospatial with the brightest UV emission of the merging companion. As no soft-energy photons are detected in the same area, this is potentially indicative of a highly obscured source. With conservative assumptions, and accounting for both background fluctuations and the extended wings of the quasar's emission, these photons only have a probability $P = 0.021$ of happening by chance. If confirmed by deeper observations, this system is the first high-redshift quasar and companion individually detected in X-rays and is likely a dual active galactic nucleus.

Unified Astronomy Thesaurus concepts: Quasar-galaxy pairs (1316); Quasars (1319); Galaxy mergers (608); Double quasars (406); X-ray astronomy (1810); X-ray quasars (1821)

1. Introduction

In recent years, the number of known quasars seen in the first billion years of the universe ($z \gtrsim 5.7$) has exploded (e.g., Venemans et al. 2015; Bañados et al. 2016; Yang et al. 2019), allowing new insights (e.g., Eilers et al. 2017; Davies et al. 2019) into the populations of the earliest supermassive black holes (SMBHs). However, explaining the formation and initial evolution of these objects remains challenging (Smith & Bromm 2019). To this end, X-ray observations of these quasars are critical, as they provide the best view of the inner regions of the active galactic nucleus (AGN) powering the quasar emission (Fabian 2016).

To date, most of the X-ray analyses of these quasars have focused on individual objects, and the current population of observed high-redshift quasars is both small and mostly only barely detected (Nanni et al. 2017; Vito et al. 2019b). Nevertheless, studies of individual quasars are still highly fruitful at characterizing mechanisms for early SMBH growth. For example, Bañados et al. (2018) showed that AGNs are already X-ray luminous at $z = 7.5$, Vito et al. (2019a) identified a heavily obscured quasar candidate in a $z = 6.5$ quasar/galaxy pair, and Nanni et al. (2018) found potential evidence of AGN variability and of jets from a $z = 6.3$ quasar.

Of particular interest is PSO J308.0416−21.2339 (hereafter PJ 308−21), a quasar at $z = 6.2341 \pm 0.0005$ discovered by Bañados et al. (2016) and whose systemic redshift is accurately measured from the [C II] emission of its host galaxy (Decarli et al. 2018). With shallow (∼10 minutes on-source) Atacama Large Millimeter Array (ALMA) observations, Decarli et al. (2017) found that the quasar has a [C II]-bright companion. Follow-up deeper and higher-resolution observations with ALMA and the *Hubble Space Telescope* (*HST*) by Decarli et al. (2019) showed that the companion is visible on both sides of the quasar, spanning over 4.″0 (20 kpc), and its kinematics can be explained by a toy model of a satellite galaxy being tidally stripped as it passes close to the quasar host galaxy. This makes PJ 308−21 one of the earliest galaxy mergers ever imaged (Decarli et al. 2019).

In this paper, we describe X-ray observations of PJ 308−21 with *Chandra*, which are among the deepest X-ray observations of a $z > 6$ quasar yet taken. One of the main objectives of our study was to see if the [C II]-bright companion could host a faint AGN; given that the first SMBHs likely grew through galaxy mergers, the chances of finding lower-luminosity AGNs are enhanced around the most distant quasars (Reines & Comastri 2016). We describe our observations in Section 2 and report the X-ray properties of the optically selected quasar in Section 3. In Section 4 we present a potential X-ray (heavily obscured) counterpart to the companion galaxy seen by ALMA and *HST*. Finally, in Section 5 we discuss our results and implications. We use a flat cosmology with $H_0 = 70$ km s^{-1} Mpc^{-1}, $\Omega_M = 0.3$, and $\Omega_\Lambda = 0.7$. We assume a Galactic absorption column density toward PJ 308−21 of $N_H = 4.02 \times 10^{20}$ cm^{-2} (Kalberla et al. 2005). We adopt a quasar redshift of $z = 6.234$; at this redshift, the scale is 5.59 kpc arcsec^{-1}. Errors are reported at the 1σ (68%) confidence level unless otherwise stated. Upper limits correspond to 3σ limits.

2. Observations and Data Reduction

We observed PJ 308−21 with the the Advanced CCD Imaging Spectrometer (ACIS; Garmire et al. 2003) on *Chandra* for a total

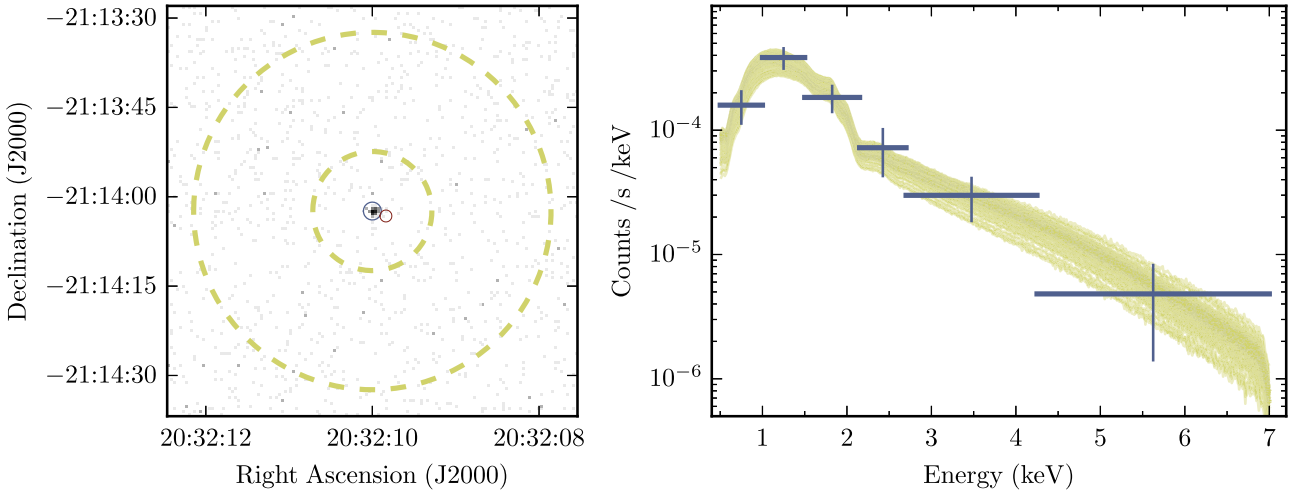

Figure 1. Left: *Chandra* observation of PJ 308−21, in the energy range 0.5–7.0 keV. The image is binned to pixels of size 0.″49, and the source and background regions are marked by a blue circle and yellow annulus, respectively. The quasar is strongly detected, and there are no other sources in the background region. We show in red the position of the candidate companion detection discussed in Section 4. Right: X-ray spectrum of PJ 308−21 (blue), with 100 well-fitting spectra underlaid (yellow). The spectrum is binned for ease of display, but fitting was performed on unbinned data. The 100 mock spectra are drawn from a Monte Carlo sampling of the fit, as described in the text.

of 150.92 ks as part of Sequence Number 703573. Observations were distributed across three visits: on 2018 August 27 (44.48 ks, Obs ID: 20470), 2018 August 29 (73.37 ks, Obs ID: 21725), and 2018 August 30 (33.07 ks, Obs ID: 21726). The detection image is shown in Figure 1. This is the second-deepest *Chandra* observation of a $z \gtrsim 6$ quasar (Nanni et al. 2018) and the third-deepest observation of this high-redshift population with either *Chandra* or *XMM-Newton* (Page et al. 2014 and Moretti et al. 2014; see Vito et al. 2019b and Pons et al. 2019 for a full list). Observations were conducted with the Very Faint telemetry format and the Timed Exposure mode, and *Chandra* was pointed so that PJ 308−21 fell on the ACIS-S3 chip. We analyzed these data using `CIAO` version 4.11 (Fruscione et al. 2006) and CALDB version 4.8.2. We used the ACIS standard filters for event grades (0, 2, 3, 4, and 6) and good time intervals. Observations were reduced with `chandra_repro` with the parameter `check_vf_pha=yes` to reduce the quiescent background.

Observations were combined using the `merge_obs` routine to create images in the broad (0.5–7.0 keV) energy band for spatial analysis. The quasar is shown in the left panel of Figure 1. For spectral analysis, we used `specextract` to extract a source spectrum from 0.5–7.0 keV (3.6–50.6 keV in the quasar rest frame) within a circular region of radius 1.″5 and a background from an annular region of inner radius 10.″0 and width 30.″0, both centered on PJ 308−21. We detect $72.3^{+9.6}_{-8.6}$ background-subtracted net counts from the source in the 0.5–7.0 keV spectral range. Spectral analysis was conducted using XSPEC v12.9.1p (Arnaud 1996) via the pyXspec utility. Due to the relatively low number of counts for Gaussian analysis (see, e.g., Arzner et al. 2007 and Humphrey et al. 2009 for further discussion), we did not bin our spectra, and used the modified C-statistic (Cash 1979; Wachter et al. 1979) to determine the best-fitting parameters. The quasar spectrum was modeled as a power law with Galactic dust absorption, using the xspec models `phabs × powerlaw`, and with rest-frame dust absorption included, using the models `zphabs × phabs×powerlaw`. The binned spectrum is shown in Figure 1.

3. Properties of PJ 308−21

We first quantified the X-ray hardness ratio[9] using the Bayesian techniques described by Park et al. (2006). We assumed uniform (Jeffreys) priors and integrated the posterior distribution with Gaussian quadrature. The hardness ratio of PJ 308−21 is $\mathcal{HR} = -0.48^{+0.11}_{-0.10}$ across the observed 0.5–2.0 keV and 2.0–7.0 keV bands. The quasar spectrum is fairly soft, in agreement with broader population trends reported by Nanni et al. (2017). Soft- and hard-band images of PJ 308−21 are shown in Figure 2.

From the best-fit of the quasar spectrum, we find that the power-law index $\Gamma = 2.39^{+0.37}_{-0.36}$ and the luminosity from 2.0 to 10.0 keV (rest frame) is $L_X = 2.31^{+1.14}_{-0.76} \times 10^{45}$ erg s^{-1} cm^{-2}. Errors were computed by evaluating the Cash statistic, C, across the distribution of model parameters for `powerlaw`; uncertainties on Γ include all values where offsets from the best-fitting Cash statistic $\Delta C \leqslant 2.30$ (two free parameters, e.g., Lampton et al. 1976). For L_X, model luminosities were computed for every set of parameters, and the reported uncertainties include all models with $\Delta C \leqslant 2.30$. As a cross-check, we also produced 100 fake spectra using the XSPEC `fakeit` command drawn from a Monte Carlo sampling of the spectral fit; these are shown in Figure 1.

We also consider the case where there is absorption at the redshift of the quasar. To do this, we modeled the emission with the xspec models `phabs × zphabs × powerlaw`. Here, `phabs` is left to the Galactic value, but `zphabs` is set to redshift $z = 6.234$, with absorbing column density $N_{H,z}$ allowed to vary. With three free parameters, the errors include all values with $\Delta C \leqslant 3.53$. For this model, we find $\Gamma = 2.8^{+1.1}_{-0.7}$, $L_X = 4.9^{+25.5}_{-3.3} \times 10^{45}$ erg s^{-1} cm^{-2} and $N_{H,z} = 2.4^{+5.5}_{-2.4} \times 10^{24}$ cm^{-2}. Unsurprisingly, $N_{H,z}$ is not well constrained, as in the high rest-frame energies we probe, variations in the spectral shape are minimal for column densities of $N_{H,z} < 10^{24}$ cm^{-2}. As including the extra term provides no meaningful constraints, and since the presence of broad lines

[9] $\mathcal{HR} = (H - S)/(H + S)$, where H and S are the net counts in the hard (2.0–7.0 keV) and soft (0.5–2.0 keV) bands, respectively.

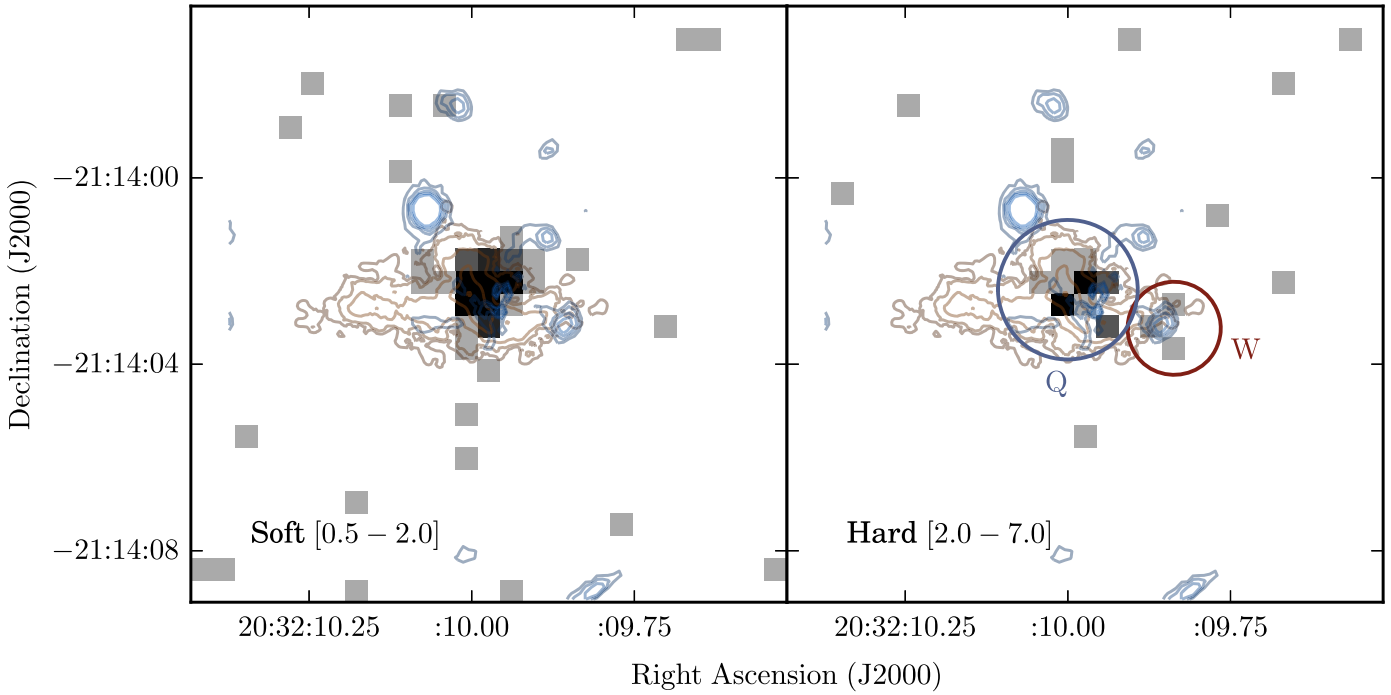

Figure 2. Grayscale image of X-ray observations of PJ 308−21, with ALMA [C II] contours (yellow) and *HST* rest-frame UV contours (blue, where the quasar has been removed through PSF subtraction) from Decarli et al. (2019) overlaid. On the left and right, the quasar is shown in the soft (0.5–2.0 keV) and hard (2.0–7.0 keV) energy bands, respectively. A faint X-ray source to the west of the quasar is seen only in the hard band, coincident with the bright UV knot "W" reported by Decarli et al. (2019). PJ 308−21 ("Q") and "W" are indicated by the blue and red circles, respectively. The bright object to the NE of the quasar in the *HST* imaging is a foreground source.

in the optical spectrum implies a column density of $N_{H,z} \lesssim 10^{22}\,\mathrm{cm}^{-2}$—which our spectrum is not sensitive to—we hereafter only consider the results when `zphabs` is not included.

Finally, we consider the X-ray-to-optical power-law slope, $\alpha_{\rm OX}$, defined as

$$\alpha_{\rm OX} = 0.3838 \times \log(L_{2\,\rm keV}/L_{2500\,\text{Å}}), \quad (1)$$

where $L_{2\,\rm keV}$ and $L_{2500\,\text{Å}}$ are the monochromatic luminosities at rest-frame 2 keV and 2500 Å, respectively. We compute $L_{2500\,\text{Å}}$ from the previously reported value of $m_{1450} = 20.46$ (Bañados et al. 2016); to make this conversion, we assume that flux in this spectral region scales as $f_\nu \propto \nu^{\alpha_\nu}$ and adopt $\alpha_\nu = -0.3$, the value used to compute m_{1450} by Bañados et al. (2016). We find $\alpha_{\rm OX} = -1.41 \pm 0.11$.

To provide further context for the properties of PJ 308−21, we also report here measurements of the quasar's black hole mass and Eddington ratio, taken from an upcoming analysis of high-redshift quasars (E. P. Farina et al. 2019, in preparation and J.-T. Schindler et al. 2019, in preparation); these results come from single-epoch virial estimators derived using the Mg II line detected in the near-infrared spectrum. They find a black hole mass of $1 \times 10^9\,M_\odot$ and an Eddington ratio of 1.5, where the statistical uncertainties are dwarfed by the roughly 0.55 dex systematic uncertainties on both quantities inherent in this technique (Onken et al. 2004; Vestergaard & Peterson 2006).

4. Potential Companions

One reason PJ 308−21 was observed was to look for X-ray counterparts to the companion first observed by Decarli et al. (2017) and later by Decarli et al. (2019). In Figure 2 we show the area around PJ 308−21 in the soft- and hard-energy bands, with the [C II] emission contours and *HST* rest-frame UV contours from Decarli et al. (2019) overplotted. While there does not appear to be any structure to the east of the quasar, three closely spaced hard X-ray photons were detected just to the west of PJ 308−21, coincident with a bright knot of stellar light observed by *HST*. These photons align with the outer extent of the [C II] emission and have no corresponding soft-band photons, highly suggestive of a heavily obscured quasar. Below, we discuss these results.

First, however, we quantify the astrometric alignment between these *Chandra* observations and the previous *HST* and ALMA observations. Using `WAVDETECT` (Freeman et al. 2002), we identify the positions of sources in our broadband image. Comparing these positions with the Guide Star Catalog v2.3 (Lasker et al. 2008) using `wcs_match`, the average residual is 0.″5, which is the size of ACIS pixels. Likewise, we compare the measured centroid of PJ 308−21 to the ALMA coordinates reported by Decarli et al. (2017). Again, we find an offset of $\lesssim$0.″5. As can be seen in Figure 2, even if our astrometry is off by 0.″5, a shift of this level will not produce a significant effect on the results discussed below.

We therefore begin our analysis with the three photons to the west. To estimate the probability that these photons arise solely from the background, we use binomial statistics to calculate probabilities, as described by Weisskopf et al. (2007) and Lansbury et al. (2014). We counted three photons within a standard 1.″0 aperture in the traditional ACIS hard-energy range (2.0–7.0 keV, e.g., Evans et al. 2010); we also extracted a background centered on our target in the same annulus used for spectroscopic analysis, finding 380 counts in the 10″–30″ aperture. We find the probability of these sources arising from the background alone to be $P = 0.013$. Similarly, we randomly

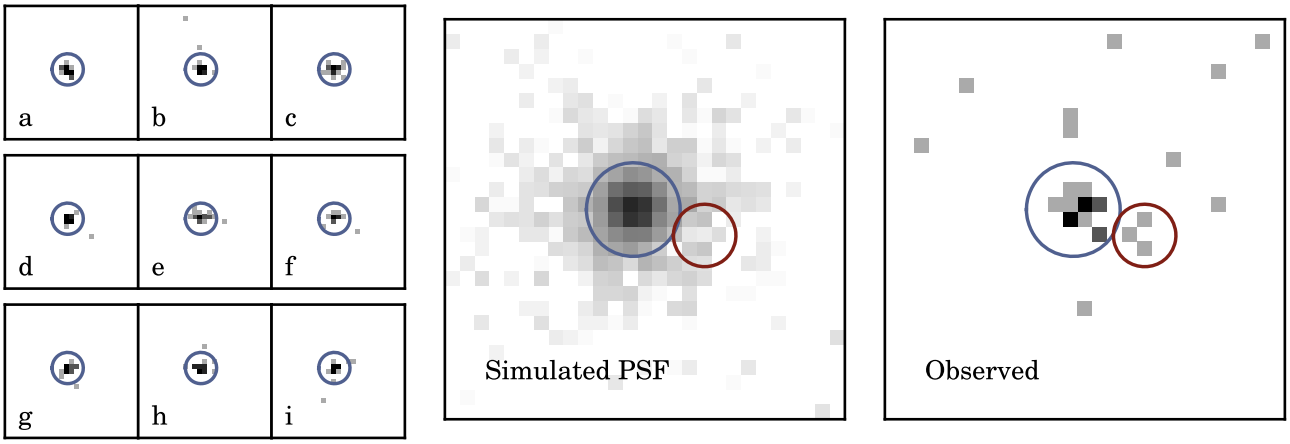

Figure 3. Comparison between the expected PSF of a single source in hard energies to the observed structure. Left: nine simulated PSFs, as described in the text, showing the same number of counts seen for the quasar and companion. Center: the summed PSF from 1000 simulations. Right: the observed hard-energy X-ray flux around PJ 308−21. All images cover the same region shown in Figure 2, and the blue and red circles show the same regions shown in that figure. The excess structure observed to the west is not consistent with being produced by the PSF alone. Note that in the central panel flux is scaled logarithmically over a larger range than in the right panel to show the extended wings of the PSF.

placed 10,000 1.″0 radius apertures in the vicinity of PJ 308−21, excluding the 5.″0 closest to the quasar, and counted the number of apertures that have at least three hard X-ray counts; from this, we estimate the probability of three counts in this small of an aperture to be $P = 0.013$.

Of course, the emission can also be influenced by the presence of the nearby X-ray bright source, PJ 308−21. In all three observations, PJ 308−21 was observed almost on-axis, such that the expected point-spread function (PSF) should be small. To better understand the expected behavior of the *Chandra* PSF, we simulated 1000 observations of a monochromatic 4 keV point source located at the position of PJ 308−21 using the *Chandra* Ray Tracer (ChaRT). These simulations provide tens of thousands of simulated photons to quantify the odds of a given photon appearing in the western region. The ChaRT output was in turn processed by marx v 5.4.0 (Davis et al. 2012) to generate synthetic PSF images. Nine of these images, which have been capped to only show the same number of counts as seen for PJ 308−21 and the candidate western companion, are shown in Figure 3, as is the full combination of all 1000 simulations. As shown in that figure, the three counts do not normally arise from the PSF; the expectation is for the PSF to only contribute 0.108 counts to the site of the potential companion, based on the flux in the inner 1.″5. Combining the effects of the PSF and the background, the probability of these three counts appearing by chance is still only $P = 0.021$.

It should be noted that we have adopted several conservative restrictions, and that by relaxing these the statistical significance could be increased—notably by using a more restricted energy range. Additionally, a fourth hard-energy photon in the companion aperture was excised through the choice to set `check_vf_pha=yes` in the original reprocessing. Use of this mode is cautioned, as it may reject real events near bright sources.[10] However, even with these conservative choices, these photons can only be explained by a random fluctuation with probability $P = 0.021$, and this detection is coincident not only with the blueshifted [C II] emission reported by Decarli et al. (2019), but also with the brightest knot of starlight identified in that work in *HST* imaging.

[10] See http://cxc.harvard.edu/ciao/why/aciscleanvf.html#real_events.

To place limits on the potential companion, we fit the observed 0.5–7.0 keV spectrum with `XSPEC`, using a `phabs × zphabs × powerlaw` model. We fixed the redshift and Galactic N_H, and evaluated the model for a series of fixed values of Γ and redshifted column density, $N_{H,z}$. The corresponding unobscured rest-frame 2.0–10.0 keV luminosities that best fit the potential companion are shown in Figure 4. In addition, we also mark the observed luminosity for PJ 308−21 and a predicted luminosity for the companion in the simplistic case that X-ray and IR luminosities are proportional. The fits show that if these photons are produced by a quasar, it must be some combination of highly shrouded, low-luminosity, or soft. We also note that, as we did not detect any photons from 0.5 to 7.0 keV for the eastern companion, any potential X-ray source associated with that region must be even fainter.

5. Discussion

While the average value of the X-ray spectral power-law index, Γ, for $z > 5.7$ quasars is $\Gamma \sim 1.9$ (Nanni et al. 2017), we found the spectrum of PJ 308−21 was best fit with a softer value, $\Gamma = 2.39^{+0.37}_{-0.36}$, which is one of the softest values for $z > 6$ quasars yet found (only considering those with reasonable constraints; Vito et al. 2019b). A number of recent works have found a correlation between Γ and the Eddington ratio (e.g., Shemmer et al. 2008; Brightman et al. 2013, 2016; this is not without some controversy though, e.g., Trakhtenbrot et al. 2017; Wang et al. 2019). Similarly, simulations (e.g., Hopkins et al. 2006) predict that major mergers drive high accretion rates in AGNs. Therefore, since this system is actively merging (Decarli et al. 2019) and accreting above the Eddington limit, the high value of Γ might be expected.

We also report on a potential detection of the gas-rich companion as a heavily obscured X-ray source. While only three counts are observed in hard X-rays, they are coincident with the extended [C II] emission and the brightest rest-frame UV knot reported by Decarli et al. (2019). Recently, Circosta et al. (2019) showed that the host galaxies of $z > 2.5$ AGNs can provide significant levels of obscuration; from the toy model for this system presented by Decarli et al. (2019), we expect to be looking through the edge-on leading edge of the companion galaxy. Adopting the simple model that the entire

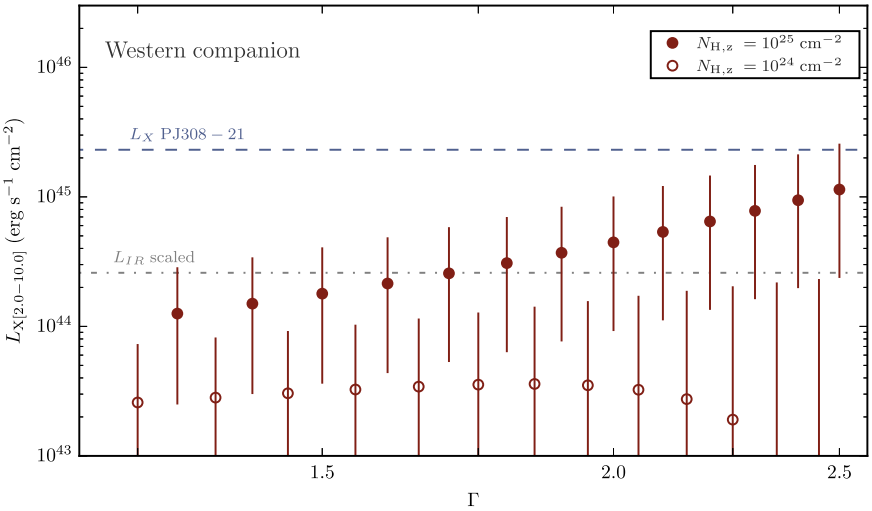

Figure 4. Best-fit luminosities with 1σ uncertainties on the unabsorbed rest-frame luminosity of the candidate obscured detection to the west of PJ 308−21 for two assumed values of rest-frame column density. The X-ray luminosity of PJ 308−21 is indicated by the dashed line. We also scale that value by the IR luminosities reported by Decarli et al. (2019) for the companion to provide a rough idea of its expected X-ray luminosities; this scaled value is marked by the dotted–dashed line. If the western region of the companion is host to a quasar, that quasar must be some combination of X-ray-faint, heavily dust-obscured, and/or have a steep power-law index.

gas mass reported by Decarli et al. (2019) for the western companion is composed of hydrogen, and adopting the Circosta et al. (2019) toy model that all the gas is in a uniform-density sphere of half-mass–radius $r_H = 1.0$ kpc, then the total column density to a source at the center of this sphere is $N_{H,z} \approx 4 \times 10^{23}$ cm^{-2}. We note both that the gas mass was measured over a larger radius than 1 kpc and that it is clearly non-uniform in density, so this column density is at best an order-of-magnitude estimate, or even an upper limit. Nevertheless, the observed gas mass could, depending on its structure and orientation, potentially contribute to the column density needed to to explain the lack of observed soft X-ray photons.

It is also worth considering PJ 308−21 in the context of PSO J167−13 ($z = 6.5$). Both quasars have [C II] bright companions (Decarli et al. 2017; Willott et al. 2017) reminiscent of ongoing mergers, and these are the only systems at redshifts $z > 6$ with companions detected in [C II] and in rest-frame UV (Decarli et al. 2019; Mazzucchelli et al. 2019; Neeleman et al. 2019). While here we report that PJ 308−21 is X-ray luminous and its companion may host a heavily obscured X-ray source, in an analysis of PSO J167−13 ($z = 6.5$) Vito et al. (2019a) reported a detection of only one source, which also appears to be heavily obscured. That these two quasars beyond $z > 6$ have both rest-frame UV-bright companions and heavily obscured quasar candidates may be consistent with the prediction of Circosta et al. (2019), that the host's interstellar medium is capable of producing significant column densities of N_H around high-redshift quasars.

The results presented here required 150 ks of observations with *Chandra*; despite this, the potentially detected companion can only be ruled out as a fluctuation to probability $P = 0.021$. This work, as well as that of Vito et al. (2019a), Bañados et al. (2018), and Nanni et al. (2018), pushes the current generation of X-ray telescopes to their limits. Future missions with high resolution and/or improved collecting areas, such as *Lynx* (Gaskin et al. 2019), *AXIS* (Mushotzky et al. 2019), and *Athena* (Nandra et al. 2013), will be necessary to advance our understanding of the earliest quasars.

We thank the anonymous referee for their productive and helpful comments. T.C. was supported by STScI/NASA award HST-GO-15198. The work of T.C. and D.S. was carried out at the Jet Propulsion Laboratory, California Institute of Technology, under a contract with NASA. The scientific results reported in this article are based on observations made by the *Chandra X-ray Observatory*. This research has made use of software provided by the *Chandra* X-ray Center (CXC) in the application package CIAO. This work is based on observations made with the NASA/ESA *Hubble Space Telescope*, obtained from the Data Archive at the Space Telescope Science Institute, which is operated by the Association of Universities for Research in Astronomy, Inc., under NASA contract NAS 5-26555. These observations are associated with program 14876. Support for this work was provided by NASA through grant No. 10747 from the Space Telescope Science Institute, which is operated by AURA, Inc., under NASA contract NAS 5-26555. This work is based on observations collected at the European Organisation for Astronomical Research in the Southern Hemisphere under ESO programme 098.B-0537(A).

Facilities: CXO, *HST*, ALMA, VLT:Kueyen.

Software: CIAO (Fruscione et al. 2006), MARX (Davis et al. 2012), XSPEC (Arnaud 1996).

ORCID iDs

Thomas Connor https://orcid.org/0000-0002-7898-7664
Eduardo Bañados https://orcid.org/0000-0002-2931-7824
Daniel Stern https://orcid.org/0000-0003-2686-9241
Roberto Decarli https://orcid.org/0000-0002-2662-8803
Jan-Torge Schindler https://orcid.org/0000-0002-4544-8242
Xiaohui Fan https://orcid.org/0000-0003-3310-0131
Emanuele Paolo Farina https://orcid.org/0000-0002-6822-2254

Chiara Mazzucchelli https://orcid.org/0000-0002-5941-5214
John S. Mulchaey https://orcid.org/0000-0003-2083-5569
Fabian Walter https://orcid.org/0000-0003-4793-7880

References

Arnaud, K. A. 1996, in ASP Conf. Ser. 101, Astronomical Data Analysis Software and Systems V, ed. G. H. Jacoby & J. Barnes (San Francisco, CA: ASP), 17
Arzner, K., Güdel, M., Briggs, K., et al. 2007, A&A, 468, 501
Bañados, E., Connor, T., Stern, D., et al. 2018, ApJL, 856, L25
Bañados, E., Venemans, B. P., Decarli, R., et al. 2016, ApJS, 227, 11
Brightman, M., Masini, A., Ballantyne, D. R., et al. 2016, ApJ, 826, 93
Brightman, M., Silverman, J. D., Mainieri, V., et al. 2013, MNRAS, 433, 2485
Cash, W. 1979, ApJ, 228, 939
Circosta, C., Vignali, C., Gilli, R., et al. 2019, A&A, 623, A172
Davies, F. B., Hennawi, J. F., & Eilers, A.-C. 2019, ApJL, 884, L19
Davis, J. E., Bautz, M. W., Dewey, D., et al. 2012, Proc. SPIE, 8443, 84431A
Decarli, R., Dotti, M., Bañados, E., et al. 2019, ApJ, 880, 157
Decarli, R., Walter, F., Venemans, B. P., et al. 2017, Natur, 545, 457
Decarli, R., Walter, F., Venemans, B. P., et al. 2018, ApJ, 854, 97
Eilers, A.-C., Davies, F. B., Hennawi, J. F., et al. 2017, ApJ, 840, 24
Evans, I. N., Primini, F. A., Glotfelty, K. J., et al. 2010, ApJS, 189, 37
Fabian, A. C. 2016, AN, 337, 375
Freeman, P. E., Kashyap, V., Rosner, R., & Lamb, D. Q. 2002, ApJS, 138, 185
Fruscione, A., McDowell, J. C., Allen, G. E., et al. 2006, Proc. SPIE, 6270, 62701V
Garmire, G. P., Bautz, M. W., Ford, P. G., Nousek, J. A., & Ricker, G. R., Jr. 2003, Proc. SPIE, 4851, 28
Gaskin, J. A., Swartz, D. A., Vikhlinin, A., et al. 2019, JATIS, 5, 021001
Hopkins, P. F., Hernquist, L., Cox, T. J., et al. 2006, ApJS, 163, 1
Humphrey, P. J., Liu, W., & Buote, D. A. 2009, ApJ, 693, 822
Kalberla, P. M. W., Burton, W. B., Hartmann, D., et al. 2005, A&A, 440, 775
Lampton, M., Margon, B., & Bowyer, S. 1976, ApJ, 208, 177
Lansbury, G. B., Alexander, D. M., Del Moro, A., et al. 2014, ApJ, 785, 17
Lasker, B. M., Lattanzi, M. G., McLean, B. J., et al. 2008, AJ, 136, 735
Mazzucchelli, C., Decarli, R., Farina, E. P., et al. 2019, ApJ, 881, 163
Moretti, A., Ballo, L., Braito, V., et al. 2014, A&A, 563, A46
Mushotzky, R. F., Aird, J., Barger, A. J., et al. 2019, arXiv:1903.04083
Nandra, K., Barret, D., Barcons, X., et al. 2013, arXiv:1306.2307
Nanni, R., Gilli, R., Vignali, C., et al. 2018, A&A, 614, A121
Nanni, R., Vignali, C., Gilli, R., Moretti, A., & Brandt, W. N. 2017, A&A, 603, A128
Neeleman, M., Bañados, E., Walter, F., et al. 2019, ApJ, 882, 10
Onken, C. A., Ferrarese, L., Merritt, D., et al. 2004, ApJ, 615, 645
Page, M. J., Simpson, C., Mortlock, D. J., et al. 2014, MNRAS, 440, L91
Park, T., Kashyap, V. L., Siemiginowska, A., et al. 2006, ApJ, 652, 610
Pons, E., McMahon, R. G., Banerji, M., & Reed, S. L. 2019, arXiv:1910.04122
Reines, A. E., & Comastri, A. 2016, PASA, 33, e054
Shemmer, O., Brandt, W. N., Netzer, H., Maiolino, R., & Kaspi, S. 2008, ApJ, 682, 81
Smith, A., & Bromm, V. 2019, ConPh, 60, 111
Trakhtenbrot, B., Ricci, C., Koss, M. J., et al. 2017, MNRAS, 470, 800
Venemans, B. P., Bañados, E., Decarli, R., et al. 2015, ApJL, 801, L11
Vestergaard, M., & Peterson, B. M. 2006, ApJ, 641, 689
Vito, F., Brandt, W. N., Bauer, F. E., et al. 2019a, A&A, 628, L6
Vito, F., Brandt, W. N., Bauer, F. E., et al. 2019b, A&A, 630, A118
Wachter, K., Leach, R., & Kellogg, E. 1979, ApJ, 230, 274
Wang, C., Yu, L.-M., Bian, W.-H., & Zhao, B.-X. 2019, MNRAS, 487, 2463
Weisskopf, M. C., Wu, K., Trimble, V., et al. 2007, ApJ, 657, 1026
Willott, C. J., Bergeron, J., & Omont, A. 2017, ApJ, 850, 108
Yang, J., Wang, F., Fan, X., et al. 2019, AJ, 157, 236